Article:
Zhang, J, Zhang, B, Li, Q et al. (4 more authors) (2022) Fast Frequency Regulation Method for Power System with Two-Stage Photovoltaic Plants. IEEE Transactions on Sustainable Energy, 13 (3). pp. 1779-1789. ISSN 1949-3029

https://doi.org/10.1109/TSTE.2022.3175662

Fast Frequency Regulation Method for Power System with Two-Stage Photovoltaic Plants

Jianhua Zhang, Bin Zhang, Qian Li, Guiping Zhou, Lei Wang, Bin Li, Kang Li

***Abstract*—The full utilization of solar energy is of great significance for reducing carbon emissions and alleviating environmental problems. Fast frequency regulation plays an important role in the power system with grid-connected two-stage photovoltaic (PV) plants. The presented fast frequency regulation method is composed of droop control, virtual inertia control and de-loading control. This work focuses on improving droop control and virtual inertia control for PV plants connected to grid. Due to non-Gaussian disturbance induced by solar irradiance, an adaptive control strategy is proposed by minimizing an improved performance index which combines mean square error (MSE) and minimum error entropy (MEE) criteria together. Based on the collected frequency deviation series data, the entropy of the frequency deviation is estimated with the aid of a quantizer. The droop control coefficient and inertia gain are then solved by an improved gravitational search algorithm (IGSA). Finally, the effectiveness of the proposed strategy is testified by an illustrative power system with a two-stage grid-connected PV plant.**

***Index Terms*—Frequency regulation, gravitational search algorithm, particle swarm optimization, photovoltaic.**

I. Introduction

ENERGY transition to carbon neutrality is of vital importance. The conventional synchronous generators will be replaced by high penetration renewable energy sources in power grid. Among various renewable energy sources, solar photovoltaic (PV) energy is regarded as one of the most promising energy sources, because it has some advantages in terms of low maintenance-cost, rapid energy conversion, long effective life, high reliability and so on [1-5].

The randomness and volatility of photovoltaic output induced by weather changes, cloud movement and other factors may arise operational and reliability problems. In addition, photovoltaic system is connected to the grid by power electronic equipment, its active power output is then decoupled from the grid frequency. With the continuous increase of photovoltaic penetration rate, frequency support capability of power systems is reduced. Even the safety and stable operation of the power grid are threatened. Control systems play important roles in maintaining the grid frequency within a proper range. In this context, it calls for investigating frequency regulation methods for the PV plants connected to power system.

Photovoltaic plants participated in frequency regulation can be classified into two kinds: PV plants equipped with or without internal energy storage systems (ESSs). For the PV plants equipped with internal ESSs, PV plants usually operate in maximum power point tracking (MPPT) mode while ESSs provide frequency response. On the other hand, the PV plants without internal ESSs usually operate in a power dispatch mode by utilizing some deliberate curtailment strategies.

When the PV plants operate in MPPT control mode, the active power of the PV plant always follows MPP. There isn't any power reserve capability to provide frequency response. Accordingly, the PV plants are usually equipped with ESSs participated in frequency regulation. At present, the PV plants without internal ESSs are also required to participate in frequency regulation, the PV plants need provide power reserves. Several de-loading control methods have been proposed to generate active power reserve. A PV plant power control strategy was proposed based on Newton's quadratic interpolation in [6], the de-loading control method was implemented by iteratively solving a quadratic polynomial. Based on a non-simplified single-diode photovoltaic model, a power-voltage characteristic fitting curve was introduced to realize de-loading control [7]. A photovoltaic system power control strategy was presented for generating active power reserve under partial shadow conditions [8].

Some research efforts have been devoted to the PV plants participated in fast frequency regulation without internal ESSs. Some virtual inertia control and droop control methods have been proposed to improve short term frequency regulation capability.

The fastest type of frequency support is inertia. The PV system can obtain inertia support capability. The research on the virtual inertia control of the grid-connected PV plants was summarized in [2-5, 9-12].

Droop control can provide fast frequency regulation. The frequency deviation of the power grid can be controlled within an allowable range by setting proper power-frequency function and fixed curtailment during normal operation and fault transients [13]. The experimental analysis indicated that the distributed voltage and the grid over-frequency can be regulated by using active power curtailment, volt-watt control and

This work was supported by National Key R&D Program of China No.2019YFB1505400. (*Corresponding author: Jianhua Zhang*)

J. H. Zhang is with the State Key Laboratory of Alternate Electrical Power System with Renewable Energy Sources, North China Electric Power University, Beijing, 102206, China (email: zjhncepu@163.com).

B. Zhang, Q. Li are with the School of Control and Computer Engineering, North China Electric Power University, Beijing, 102206, China.

G. P. Zhou, L. Wang and B. Li are with the State Grid Liaoning Electric Power Supply Co. Ltd., Shenyang, 110006, China.

K. Li is with School of Electronic and Electric Engineering, University of Leeds, LS2 9JT, UK.

frequency-watt control together [14]. A droop control method was proposed for the PV plants to provide primary frequency support, moreover, an emergency controller can be switched to prevent system frequency collapse in case of severe faults. A frequency regulation scheme was designed for PV plants without internal ESSs after the active power curtailment had been realized [15]. Nevertheless, the droop controller with a fixed slope and a pre-defined dead band were adopted in [13-15]. To improve primary frequency response, the droop coefficient can be continuously adjusted in response to varying solar irradiance.

In addition, virtual inertia control and droop control have been combined to modify the reference value of photovoltaic active power, the PV plants can regulate frequency quickly [16-18]. A two-stage grid-connected PV system with frequency response capabilities was investigated, the droop controller reduces the maximum frequency excursions while the inertia controller increases the system inertia [19]. A fast frequency regulation scheme was designed for a PV system, in which both droop controller and virtual inertia controller were applied to provide frequency support [20]. A de-loading fuzzy controller and a control mode selector were presented for PV plants, the fuzzy controller that comprises droop control and inertia control improved the frequency regulation quality [21].

The aforementioned control methods are based on system models. Model-free or data-driven method is an alternative way to realize flexible control in practice. In [22-24], three novel adaptive dynamic programming based learning algorithms were developed for load frequency control in power systems [22], ESSs based frequency control systems [23] and electric vehicles based frequency control systems, respectively [24]. A model-free fast frequency control was presented to realize ESSs based frequency support [25]. Few references have focused on model-free or data-driven frequency control strategy for PV plants so far. The objective functions used in the above data-driven frequency control strategies [21-25] can not necessarily deal with non-Gaussian disturbance induced by solar irradiance. It is necessary to investigate data-driven frequency regulation under a stochastic framework.

The challenges in fast frequency regulation of PV plants without ESSs are exhibited as:

(1) For grid-connected PV systems, their accurate models are not easy to be obtained using physical principles.

(2) It calls for a proper control objective to deal with solar irradiance disturbance when designing data-driven frequency control strategy.

(3) An optimization approach is needed to solve data-driven frequency control problem since there isn't enough information to mathematically formulate the PV frequency control problem.

Minimum error entropy (MEE) has become an important criterion for non-Gaussian systems instead of mean square error (MSE), which is usually used to design controller and filter for nonlinear and non-Gaussian systems [26-28]. Meanwhile, some non-exact innovative optimization approaches have been presented to solve complicated optimization problems [29-32].

Motivated by these investigations, an adaptive control strategy is proposed for a two-stage grid-connected PV plant participating in frequency regulation. The novelties and contributions are briefly summarized as:

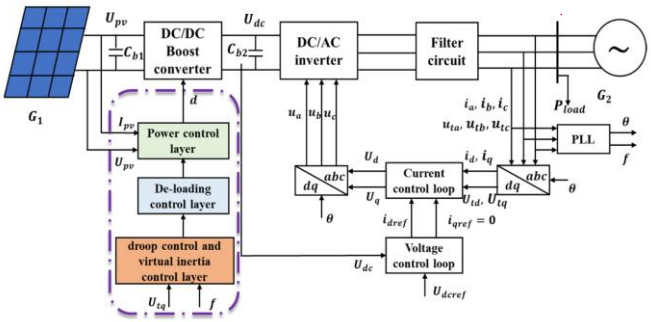

Fig. 1. Frequency control system of a two-stage grid-connected PV plant.

The novelties and contributions are briefly summarized as:

(1) An integrated frequency regulation scheme is presented for two-stage PV plants by combining droop control, virtual inertia control and de-loading control together.

(2) A data-driven droop and inertia control method is proposed under a stochastic framework, MEE and MSE criteria are employed to formulate the frequency control objective;

(3) The optimal droop and inertia control algorithm is solved by combing gravitational search algorithm (GSA) and particle swarm optimization (PSO) technique;

(4) Comparative simulation results verify the superiority of the proposed adaptive control strategy.

This paper is organized as follows. In Section II, a fast frequency regulation strategy is presented for a two-stage grid-connected PV plant. Section III introduces the proposed adaptive control method in detail. Section IV discusses the simulation results of the proposed integrated frequency regulation strategy with the adaptive control algorithm. Finally, Section V presents conclusions drawn from the simulation results.

II. Fast Frequency Regulation Strategy of PV Power Plant

In order to provide frequency response for the grid-connected PV plants, the active power reserve is required. Besides, a combination of virtual inertia control and droop control can provide inertia and primary frequency support. Hence, a fast frequency regulation strategy shown in Fig. 1 is presented for a two-stage grid-connected PV plant, where G_1 and G_2 stand for the PV plant and the thermal power plant respectively. U_{pv} and I_{pv} are the output voltage and current of the PV plant respectively. C_{b1} and C_{b2} represent the capacitors on both sides of the DC/DC boost converter. f, d and θ are frequency, cycle and phase respectively. U_{dc} and U_{dcref} represent the DC bus voltage and its reference voltage respectively. i_a, i_b and i_c are three-phase AC current; u_{ta}, u_{tb} and u_{tc} stand for three-phase AC voltage; i_d, i_q, U_{td} and U_{tq} are current and voltage in dq coordinate system respectively; i_{dref} and i_{qref} represent the reference currents in dq coordinate system respectively; U_d and U_q stand for the control signals in dq coordinate system respectively; u_a, u_b and u_c are three-phase AC control signal respectively.

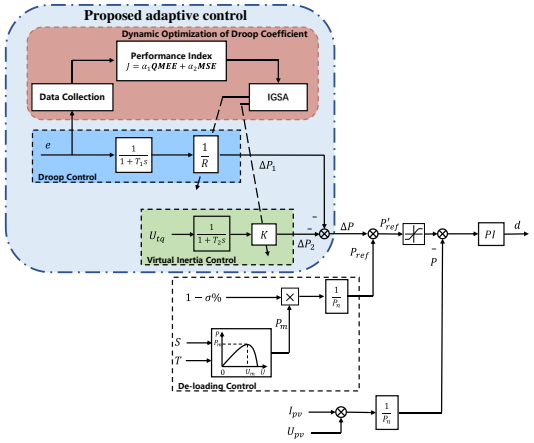

Fig. 2. Integrated frequency control.

The DC/AC inverter side includes a voltage control loop and a current control loop, where the voltage control loop maintains the stability of the DC bus voltage U_{dc} while the current control loop generates corresponding control signals to implement the inverter process.

As shown in Fig. 1, the frequency regulation scheme adopts a hierarchical control strategy to implement fast frequency regulation for grid-connected two-stage PV plants. e is the frequency deviation. The presented hierarchical control strategy mainly focuses on the DC/DC boost converter side. Figure 2 illustrates the integrated frequency regulation scheme in detail. It comprises the droop control and virtual inertia control layer, de-loading control layer and power control layer.

In the droop control and virtual inertia control layer, the output active power of the PV plant is controlled according to the frequency deviation and the rate of change of frequency (ROCOF), the corrected power reference value ΔP can then be obtained, consequently, the PV plant can achieve frequency regulation response like a synchronous generator. In the de-loading control layer, the PV plant obtains a certain amount of power reserve. The duty cycle d generated from the power control layer drives the DC/DC boost converter to adjust the output voltage of the PV plant U_{pv}, as a result, the output power of the PV plant P tracks its reference P'_{ref}.

A. *De-loading Control*

De-loading control is applied to provide active power reserve for the investigated PV plant. Considering the volatility and randomness existed in the PV plants, solar irradiance is introduced to set the de-loading ratio $\sigma\%$ for alleviating the grid frequency deviation [33].

$$\sigma\% = \sigma_0\% * S/S_{ref} \tag{1}$$

where $\sigma_0\%$ is the initial de-loading ratio, S stands for solar irradiance, $S_{ref} = 1000W/m^2$ represents the reference value of solar irradiance at standard test condition (STC).

Hence, the output power of the PV plant in de-loading mode is

$$P_{ref} = [P_m(1-\sigma\%)]/P_n \tag{2}$$

where P_m is the maximum output power of the PV plant, which can be estimated by [34]

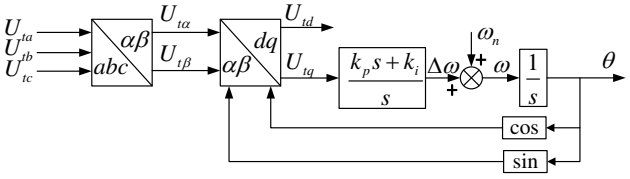

Fig. 3. Control diagram of PLL.

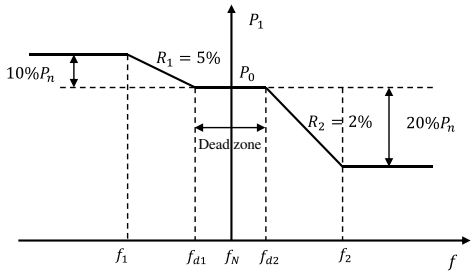

Fig. 4. Droop control curve of PV plant.

$$\begin{aligned} P_m &= U_m I_m \\ U_m &= U_m(S,T) = a_1(S-b_1)^2 + c(T_{ref}-T) + d \\ I_m &= I_m(S,T) = a_2 S + b_2\left(T - T_{ref}\right)S \end{aligned} \tag{3}$$

where $T_{ref} = 25^{\circ}\mathrm{C}$ is the temperature at STC. U_m and I_m are the maximum power point voltage and current. The parameters are set to $a_1 = 4.4 \times 10^{-6}$, $b_1 = 638.25$, $c = 0.0504$, $d = 16.918$, $a_2 = 8.58 \times 10^{-3}$ and $b_2 = 2.145 \times 10^{-5}$, respectively.

B. *Virtual Inertia Control*

The ROCOF can be introduced to regulate frequency by injecting or absorbing active power into/from the system instantaneously. Based on the grid code for auxiliary service management for grid-connected power plants in the northeast China power grid, the virtual inertia response of the PV plant should satisfy

$$\Delta P_{PV} \approx -\frac{T_J}{f_N}\frac{df}{dt}P_n \tag{4}$$

where the virtual inertia response time constant of the PV plants T_J is set to 4~20s generally. f_N and P_n are the rated frequency and power of the PV plant respectively.

Based on the phase locked loop (PLL) control system, the frequency can be formulated to read

$$f = \frac{U_{tq}}{2\pi}\left(k_p + \int k_i dt\right) \tag{5}$$

where k_p and k_i are the proportional and integral coefficients of the PI controller respectively. The derivative of the frequency can be expressed by

$$\frac{df}{dt} = \frac{U_{tq}k_{i4}}{2\pi} \tag{6}$$

Substituting (6) to (4), the variation of the active power induced by virtual inertia control can be described as follows

$$\Delta P_{PV} = -\frac{T_J}{f_N}\frac{U_{tq}k_{i4}}{2\pi}P_n = -K * U_{tq} \tag{7}$$

where K is the virtual inertia coefficient. The virtual inertia control ΔP_2 can be implemented by

$$\Delta P_2 = -K * U_{tq} * \frac{1}{1+T_2 s} \tag{8}$$

where a low-pass filter is used to eliminate the noise of U_{tq}.

C. Droop Control

Droop control is a commonly used primary frequency regulation control strategy. A low-pass filter whose time constant T_1 is used to eliminate the noise of the frequency deviation. As shown in Fig. 4, there are several parameters that determine the droop curve characteristic in term of the droop up and droop down slopes, dead band and power ramp rate.

When the PV plant participates in primary frequency regulation, the parameters related to the droop curve characteristic shown in Fig. 4 are set according to the grid code for grid-connected power plants in the northeast China power grid [36]. The power reduction range should not be less than $20\%P_n$, the droop up coefficient is R_2 =2% for over-frequency response; The power ascending range should not be less than $10\%P_n$, and the droop down coefficient is R_1 =5% for under-frequency response.

$$\Delta P_1 = P_1 - P_0 = \begin{cases} -\dfrac{1}{R_2} \times (f - f_{d2}) & f_{d2} < f < f_2 \\ 0 & f_{d1} < f < f_{d2} \\ -\dfrac{1}{R_1} \times (f - f_{d1}) & f_1 < f < f_{d1} \end{cases} \quad (9)$$

where $f_{d1} = 49.95\text{Hz}$ and $f_{d2} = 50.05\text{Hz}$ determine the frequency dead zone. R_1 and R_2 represent the droop down and droop up coefficients, respectively.

Although the traditional droop controller and inertia controller can provide additional active power based on the grid frequency deviation and ROCOF, the adaptive control algorithm can obtain better primary frequency regulation performance. An improved control method will be presented in Section III.

III. An Adaptive Control Strategy

In this section, an adaptive control shown in Fig. 2 is proposed for the grid-connected two-stage PV plant instead of the traditional inertia and droop controllers described by Eq. (8) and Eq. (9). The slope of the droop curve and the inertia gain under adaptive control will be tuned in real-time by solving a multi-objective optimal problem.

A. Improved Performance Index

The distribution of solar irradiance is usually non-Gaussian, so is the frequency deviation of the power system with renewable energy sources. Naturally, the adaptive droop control coefficient and the inertia gain should be solved under the stochastic framework. The MEE criterion can ensure the probability density function (PDF) of the frequency deviation , $p(e)$, approach to a narrowly shaped normal distribution, however, its Renyi entropy of $\alpha(\alpha > 0, \alpha \neq 1)$ order, $H_\alpha(e)$, has the shift-invariance property. As a result, the adaptive droop coefficient and the inertia gain can be solved by minimizing following performance index that combines MSE and MEE criteria.

$$J = \alpha_1 H_\alpha(e) + \alpha_2 E(e^2) \quad (10)$$

where α_1 is the weight to the entropy of the frequency deviation, α_2 the weight to the mean value of the squared frequency deviation.

Let $\alpha = 2$. Since minimizing quadratic Renyi entropy $H_2(e)$ is equivalent to minimizing the inverse of the quadratic information potential $I_2(e)$, the performance index (10) can be reformulated as

$$J = \alpha_1 \frac{1}{I_2(e)} + \alpha_2 E(e^2) \quad (11)$$

The PDF of the frequency deviation, $p(e)$, can be estimated using the Parzen window technique

$$\hat{p}(e) = \frac{1}{N} \sum_{j=1}^{N} G_\sigma(e - e_j) \quad (12)$$

where the frequency deviation series $\{e_1, e_2, e_3 \dots e_N\}$ are collected within the sliding window whose width is N. The kernel function with kernel width σ is $G_\sigma(x) = \frac{1}{\sqrt{2\pi}\sigma} exp\left(-\frac{x^2}{2\sigma^2}\right)$. The quadratic information potential can then be calculated by

$$\hat{I}_2(e) = \frac{1}{N} \sum_{i=1}^{N} \hat{p}(e) = \frac{1}{N^2} \sum_{i=1}^{N} \sum_{j=1}^{N} G_\sigma(e_i - e_j) \quad (13)$$

It can be seen from (13) that two sums are required to calculate the quadratic information potential, and the computational complexity is $o(N^2)$. Hence, a quantizer is employed to estimate the quadratic information potential for reducing computational burden [28]. Denoting $Q[\cdot]$ as a quantizer with a codebook $C = \{c_1, c_2, c_3 \dots c_M\}$ that contains $M(M \leq N)$ real-valued code words, the quantizer $Q[\cdot]$ can map the frequency deviation series $e = \{e_1, e_2, e_3 \dots e_N\}$ into one of the M code words in C. In this work, each frequency deviation series is quantized to the nearest code word, the quantized quadratic information potential can then be estimated

$$\begin{aligned} \hat{I}_2^Q(e) &= \frac{1}{N^2} \sum_{i=1}^{N} \sum_{j=1}^{N} G_\sigma(e_i - Q[e_j]) \\ &= \frac{1}{N^2} \sum_{i=1}^{N} \left(\sum_{m=1}^{M} M_m G_\sigma(e_i - c_m) \right) \end{aligned} \quad (14)$$

where M_m is the length of the frequency deviation series, which can be represented by the m_{th} element in the codebook. Obviously, when $M = N$, $\sum_{m=1}^{M} M_m = N$.

It is clear from (14) that the computational complexity of the quantized quadratic information potential is simplified from $o(N^2)$ to $o(NM)$.

The adaptive droop coefficient and the inertia gain can be obtained by minimizing the following performance index

$$J = \alpha_1 \frac{1}{\hat{I}_2^Q(e)} + \alpha_2 E(e^2) \quad (15)$$

It is worth noting that the measured frequency implies the information of all stochastic disturbances, such as solar irradiance disturbance, measurement noise, load disturbance and so on. It means that the performance index (15) owns abundant statistical characteristics of the frequency deviation.

B. IGSA

In order to obtain adaptive droop coefficient and inertia gain by minimizing the performance index (15), an improved gravitational search algorithm (IGSA) is applied to solve the optimal problem by combing particle swarm optimization

(PSO) technique and gravitational search algorithm (GSA).

Gravitational search algorithm has been applied to solve optimal problems [30-32]. Every object attracts other objects with a gravitational force.

The force leads to a global movement of all objects toward the objects with heavier masses. The optimal solution is the position of the object with heaviest mass.

It is assumed that there are N objects in a D-dimensional search space. The position of the i_{th} object is defined as follows

$$x_i = \left(x_i^1, x_i^2 \cdots, x_i^d, \cdots, x_i^D\right), i = 1,2, \cdots, N \quad (16)$$

where x_i^d represents the position of the i_{th} object in the d_{th} dimension.

At time t, a gravitational force $F_{ij}^d(t)$ from the j_{th} object acting on the i_{th} object is specified as:

$$F_{ij}^d(t) = G(t)\frac{M_{pi}(t) + M_{aj}(t)}{R_{ij}(t) + \varepsilon}\left(x_j^d(t) - x_i^d(t)\right) \quad (17)$$

where M_{aj} and M_{pi} are the active mass of object j and the passive mass of object i respectively. ε is a constant. x_i^d and x_j^d are the position components of objects i and object j in the d_{th} dimension, respectively. The gravitational constant at time t, $G(t)$, can be calculated by

$$G(t) = G_0 \times e^{-\frac{\alpha t}{T}} \quad (18)$$

where T stands for the total number of iterations. α is an adjustable parameter which controls the convergence speed of the algorithm. The gravitational constant at the initial moment, G_0, is determined according to the range of the search space. The Euclidean distance between the i_{th} object and the j_{th} object, $R_{ij}(t)$, is defined by

$$R_{ij}(t) = \left\|x_i(t), x_j(t)\right\|_2 \quad (19)$$

A stochastic characteristic is introduced to GSA, the total force acting on the i_{th} object is calculated by a randomly weighted sum of the forces imposed by other objects.

$$F_i^d(t) = \sum_{j=1, j\neq i}^{N} rand_j F_{ij}^d(t) \quad (20)$$

where $rand_j$ is a random number uniformly distributed over the interval of [0, 1].

According to Newton's second theorem, the acceleration $a_i^d(t)$ of the i_{th} object on the d_{th} dimension at time t is given by

$$a_i^d(t) = \frac{F_i^d(t)}{M_{ii}(t)} \quad (21)$$

where M_{ii} is the inertial mass of the i_{th} object.

In order to simplify the computation of masses, let the active and passive gravitational masses be equal to the inertial mass

$$M_{ai}(t) = M_{pi}(t) = M_{ii}(t) = M_i(t), i = 1,2, \cdots, N \quad (22)$$

The normalized mass inertial mass of the objects can be described by

$$M_i(t) = \frac{m_i(t)}{\sum_{j=1}^{N} m_j(t)} \quad (23)$$

where the inertial mass of the i_{th} object is defined as follows

$$m_i(t) = \frac{fit_i(t) - worst(t)}{best(t) - worst(t)} \quad (24)$$

where $fit_i(t)$ represents the fitness value of the i_{th} object at time t. $worst(t)$ is the worst fitness value in the population. $best(t)$ stands for the best fitness value in the population. In order to solve the optimal droop coefficient and inertia gain by minimizing the fitness (15), $worst(t)$ and $best(t)$ are defined as follows:

$$\begin{cases} best(t) = min_{j\in\{1,2,\cdots,N\}} fit_j(t) \\ worst(t) = max_{j\in\{1,2,\cdots,N\}} fit_j(t) \end{cases} \quad (25)$$

The velocity and the position are then updated based on the classical mechanics

$$v_i^d(t+1) = rand_i \times v_i^d(t) + a_i^d(t) \quad (26)$$

$$x_i^d(t+1) = x_i^d(t) + v_i^d(t+1) \quad (27)$$

It can be seen from (26) and (27) that the updating rules of GSA only use current velocity and position of the object. Unlike GSA, PSO utilizes memory and social information [36]. Hence, the updating rules of the object's velocity GSA can be improved by introducing the following updating rule of the particle's velocity shown in PSO algorithm

$$v_i^d(t+1) = v_i^d(t) + c_1 rand_1\left[p_{best}^d - x_i^d(t)\right] + c_2 rand_2\left[g_{best}^d - x_i^d(t)\right] \quad (28)$$

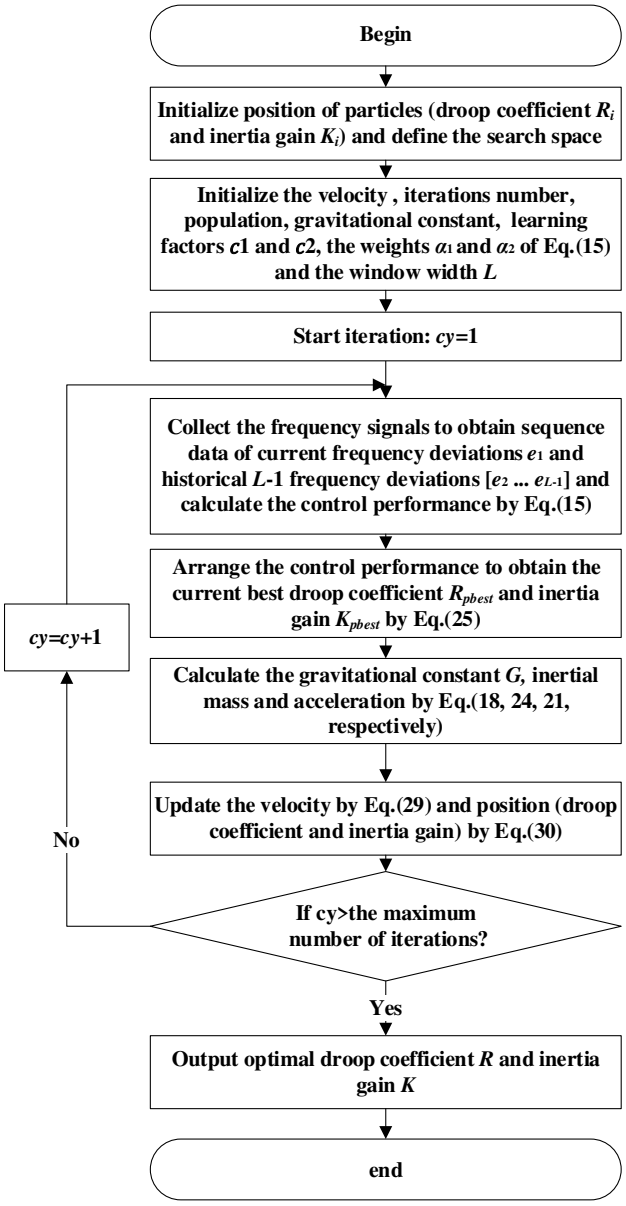

Fig. 5. Coordinate control of PV plant using IGSA.

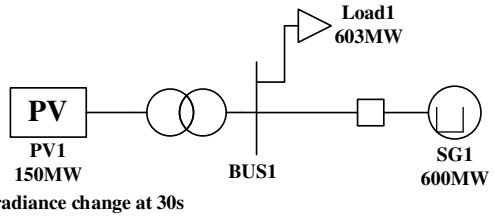

Fig. 6. Simulated power system.

TABLE I
PARAMETERS OF THE POWER SYSTEM AND OPTIMAL METHODS

Parameter	Value
Power of thermal power plant	600MW
Power of photovoltaic power plant	150MW
Value of initial load	603MW
Initial de-loading ratio	20%
Population size	100
Number of iterations	80
Initial value of gravitational constant G_0	50
Learning factor c_1	0.5
Learning factor c_2	0.5
QMEE's weight α_1	0.4
MSE's weight α_2	0.6
Width of sliding window N	100
Virtual inertia control gain K	10
Droop down coefficient	0.05
Droop up coefficient	0.02
Sampling period	5e-5s
Time constant T_1	1s
Time constant T_2	2s

where c_1 and c_2 are learning factors, $rand_1$ and $rand_2$ are random numbers in the range of [0,1].

The velocity (26) can then be updated by

$$v_i^d(t+1) = c_1 rand_1\left[x_{pbest}^d(t) - x_i^d(t)\right] + c_2 rand_2\left[x_{gbest}^d(t) - x_i^d(t)\right] + rand_3 v_i^d(t) + a_i^d(t) \quad (29)$$

where $rand_3$ is also a random number within the range of [0,1]. $x_{pbest}^d(t)$ is the best previous position that the i_{th} object has ever reached until time t. $x_{gbest}^d(t)$ represents the previous best global position.

The position is still updated based on the classical mechanics

$$x_i^d(t+1) = x_i^d(t) + v_i^d(t+1) \quad (30)$$

The reasons to enhance the effectiveness of IGSA lie in: 1) the integrated PSO uses a memory $(pbest, gbest)$ to save the position found so far; 2) Each particle can find the best solution $(pbest, gbest)$ and moves towards it; 3) All particles move slowly when they approach to a good solution, $gbest$ can help them to exploit the global best; 4) IGSA utilizes the fitness value to adjust the accelerations.

The flow chart of the IGSA based coordinate control method is shown in Fig. 5.

IV. SIMULATION RESULTS

In this section, some simulations are conducted to testify the effectiveness of the proposed frequency control strategy. The proposed fast frequency regulation scheme shown in Fig. 2 is applied to the simulated power system depicted in Fig. 6. The

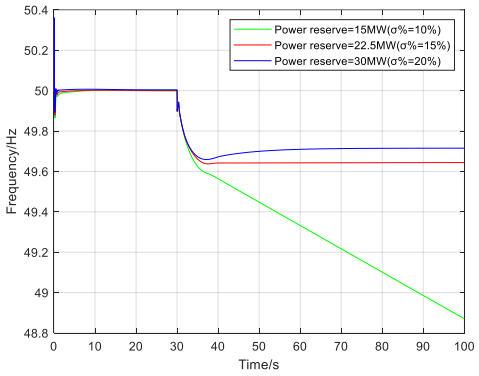

Fig. 7. Impacts on frequency response.

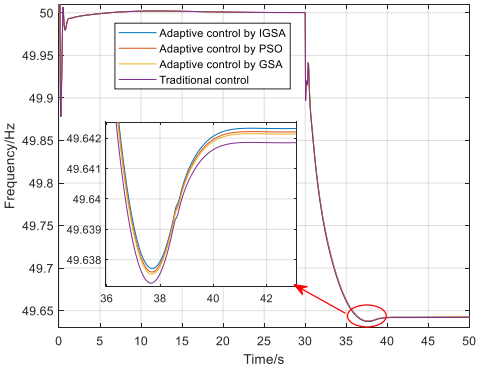

Fig. 8. System frequency response. ($\sigma\% = 15\%$)

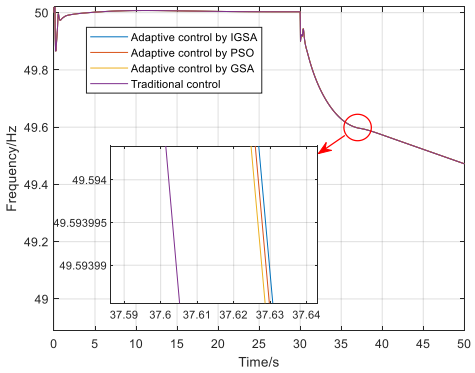

Fig. 9. System frequency response. ($\sigma\% = 10\%$)

parameters of the PV Plant and optimal methods are listed in Table.1.

De-loading control strategies are same during comparative investigations. The traditional droop and inertia control is compared with the proposed adaptive control. When the PV plant uses the traditional additional frequency control, the inertia gain is set to $K = 10$, the droop up coefficient is $R_2 = 2\%$ for over-frequency response while the droop down coefficient $R_1 = 5\%$ for under-frequency response.

The simulation tests are classified into three scenarios. The amount of power reserves and their impacts on frequency response are analyzed in Scenario 1. There isn't any stochastic disturbance imposed on solar irradiance in Scenario 2, whereas a non-Gaussian disturbance is imposed on solar irradiance in Scenario 3.

Scenario 1: Impacts of power reserves

A positive step of load, 73MW, is imposed at 30s in following cases.

Case 1: The effect of power reserves on frequency stability under the proposed IGSA based frequency control method is investigated. When power reserves are 15MW ($\sigma\% = 10\%$), 22.5MW ($\sigma\% = 15\%$) and 30MW ($\sigma\% = 20\%$) respectively, the system frequency responses are shown in Fig. 7. It can be observed that the frequency control performance deteriorates with decreasing power reserves. The nadir becomes lower and the steady frequency deviates from 50Hz greatly when reducing power reserves.

Case 2: When power reserve is 22.5MW, Fig. 8 plots the frequency profiles under four control methods after load disturbance. It is clear that the frequency nadir and the steady frequency under the proposed control are the largest, hence, the proposed control method is superior to other three control methods.

Case 3: When power reserves is 15MW, the system frequency response is shown in Fig. 9. The frequency is unstable under four control methods, since power reserve is insufficient to prevent frequency nadir from going down.

Scenario 2: Solar irradiance without stochastic disturbance

Solar irradiance and the temperature are set to 1000W/m^2 and 25℃ respectively. The system load is increased by 60MW at 30s.

Variations of droop coefficients and inertia gains are displayed in Fig. 10 (a) and Fig. 10 (b), respectively. Responses of system frequency and ROCOF under the proposed IGSA based frequency regulation are shown in Fig. 10 (c) and Fig. 10 (d), respectively. The droop coefficient under the proposed control is the largest, as a result, the steady frequency is closest to 50Hz.

When the adaptive control methods are adopted based on IGSA, GSA and PSO, respectively, it can be observed from Fig. 10 (c) that the frequency nadirs are 49.7455 Hz, 49.7365Hz and 49.7323Hz, respectively; the steady frequency are 49.8145 Hz, 49.81Hz and 49.8079Hz, respectively. On the other hand, the frequency nadir and the steady-state frequency value under the traditional control are 49.7169 Hz and 49.7951Hz, respectively. Obviously, the proposed IGSA based frequency controller drives the frequency response to reach its nadir earlier than other controllers.

As shown in Fig. 10 (b) and Fig. 10 (d), the proposed IGSA based frequency regulation method is more effective to attenuate the ROCOF due to the larger inertia constant at the early stage of the incident.

The active power of the PV plant under four kinds of control is compared and displayed in Fig. 11 (a). The additional PV power reference $\Delta p = \Delta p_1 + \Delta p_2$ introduced for the droop control and inertia control is shown in Fig. 11 (b). The proposed IGSA based frequency control method can obtain the largest additional PV power reference, consequently, the PV plant generates most power. It means that the proposed IGSA based frequency controller can bring most economic benefits.

The frequency control evaluating metrics include root mean square error (RMSE), mean absolute error (MAE), MSE, mean absolute percent error (MAPE) and standard deviation (SD).

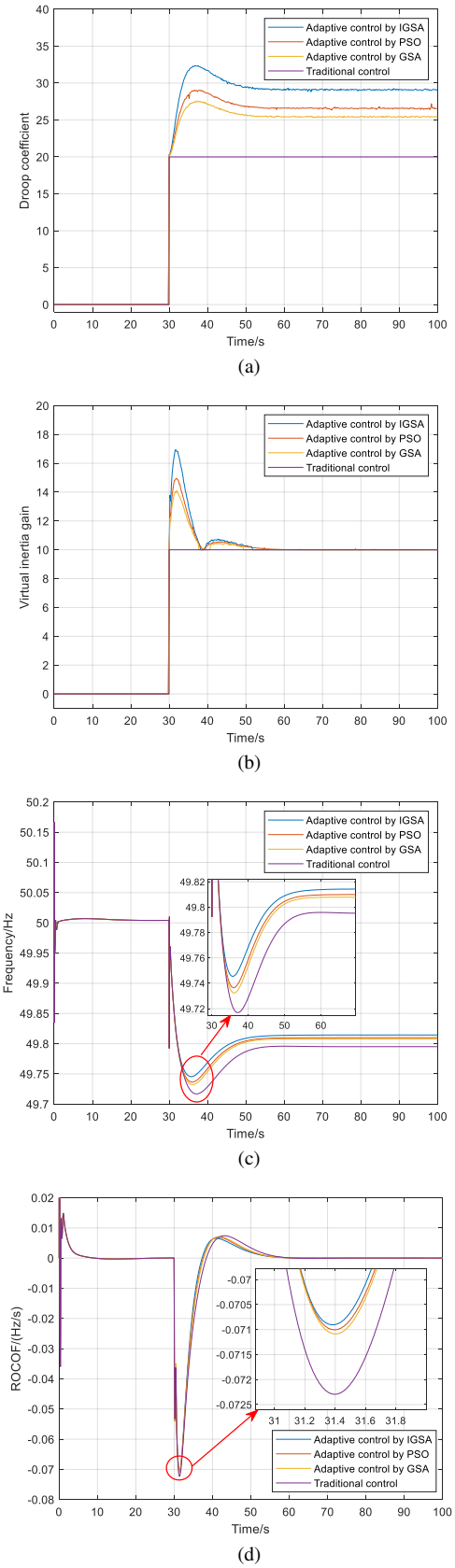

Fig. 10. Comparative results of 4 different control strategies in Scenario 2. (a) Droop coefficients. (b) Virtual inertia gains. (c) System frequency response. (d) Instantaneous ROCOF.

The radar chart exhibited in Fig. 12 is introduced for visualizing

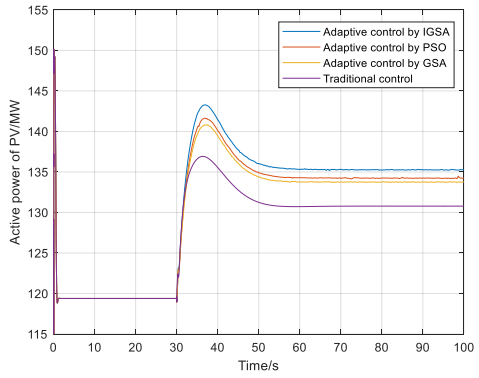

(a)

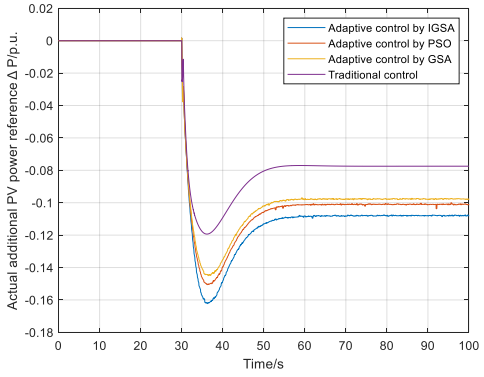

(b)

Fig. 11. Comparative results of 4 different control strategies in Scenario 2. (a) Active power. (b) Actual additional PV power reference.

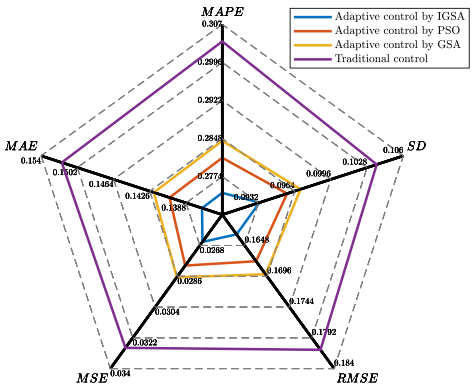

Fig. 12. Frequency control evaluating metrics.

the statistic results of these evaluating metrics. The IGSA based adaptive control method can achieve best frequency regulation performance, the narrower radar-shadow and smaller covered area indicate smaller frequency deviation.

Figures 10 (c) and 12 reveal the superiorities of proposed adaptive control method, which can significantly improve the frequency regulation quality.

Scenario 3: Non-Gaussian disturbance is imposed to solar irradiance

In this test, the temperature is still set to 25℃, a beta distribution is used to describe the PDF of short-term solar irradiance [37]. The solar irradiance is shown in Fig. 13 (a). Figure 13 (b) presents the test result of normal probability distribution based on the solar irradiance data displayed in Fig. 13 (a). It can be found that the logarithmic diagram of the

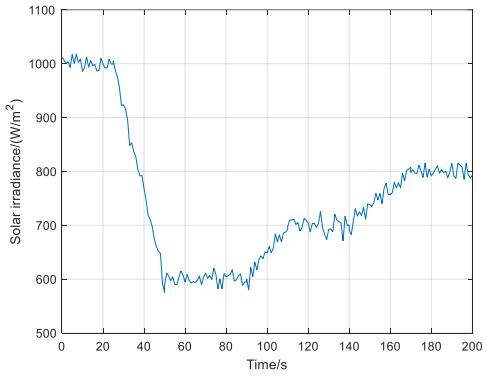

(a)

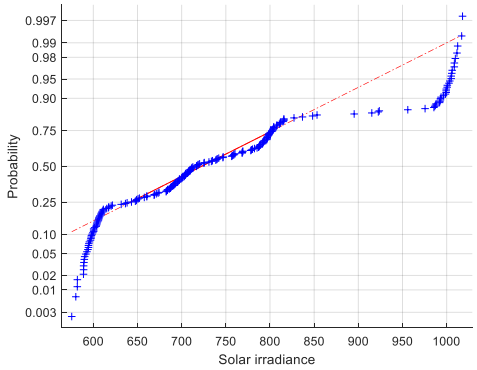

(b)

Fig. 13. Solar irradiance in Scenario 3. (a) Solar irradiance. (b) Normal probability distribution test of Solar irradiance.

probability density function (PDF) of solar irradiance is not linear, hence, solar irradiance is non-Gaussian.

The comparative droop coefficients and inertia gains are displayed in Fig. 14 (a) and Fig. 14 (b), respectively. Figures 14 (c) and 14 (d) show system frequency and ROCOF profiles respectively. It is clear from Fig. 14 (a) that droop coefficient under the proposed IGSA based frequency control is always greatest, as a sequence, the quasi-steady frequency is also greatest as shown in Fig. 14 (c). In addition, the nadir is greater using the adaptive control algorithm. Figures 14 (d) demonstrates that the proposed IGSA based frequency control method can obtain better ROCOF response due to its inertia gain shown in Fig. 14 (b).

Fig. 15 (a) show the active power during the test. The additional power reference of the PV plant is compared and displayed in Fig. 15 (b). It can be seen from Fig. 15 (a) and Fig. 15 (b) that photovoltaic generates most power under the IGSA based adaptive control method, which obtains the best economic benefits.

The radar chart shown in Fig. 16 demonstrates that the IGSA based adaptive control method can achieve best frequency regulation performance according to different evaluating metrics.

V. Conclusions

This paper proposed an integrated frequency regulation scheme for two-stage grid-connected PV plants. It includes the

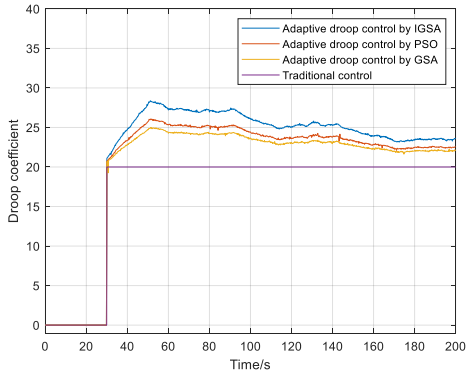

(a)

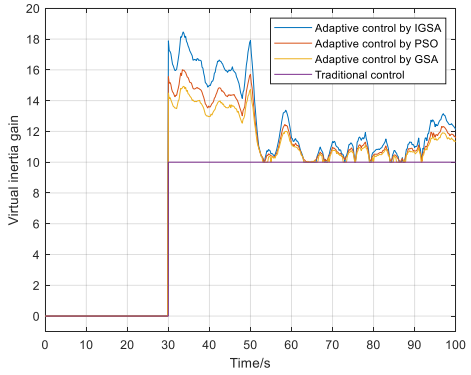

(b)

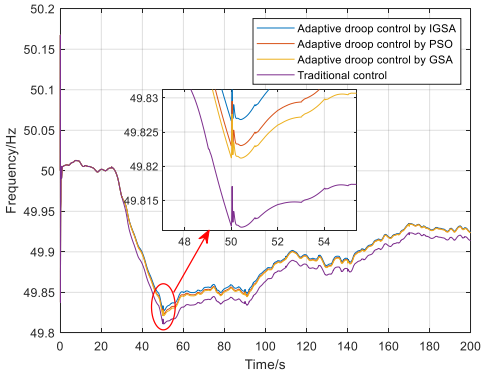

(c)

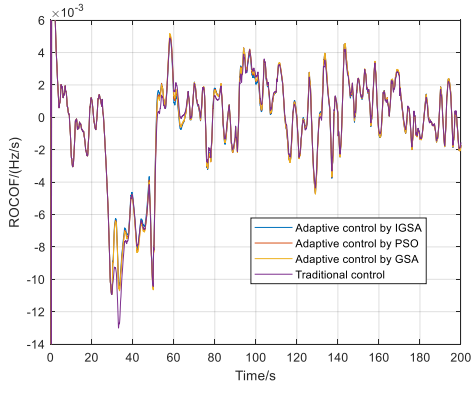

(d)

Fig. 14. Comparative results of 4 different control strategies in Scenario 3. (a) Droop coefficients. (b) Virtual inertia gains. (c) System frequency response. (d) Instantaneous ROCOF.

droop control and virtual inertia control layer, de-loading

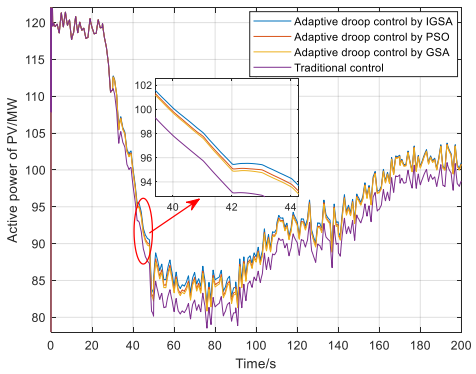

(a)

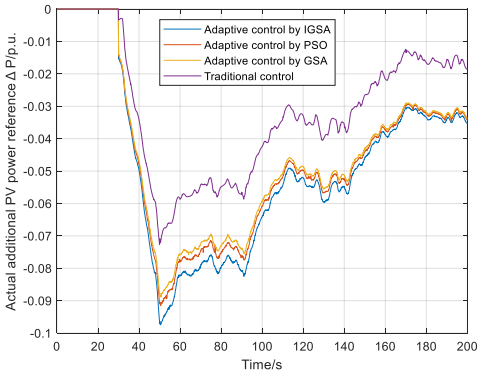

(b)

Fig. 15. Comparative results of 4 different control strategies in Scenario 3. (a) Active power. (b) Actual additional PV power reference.

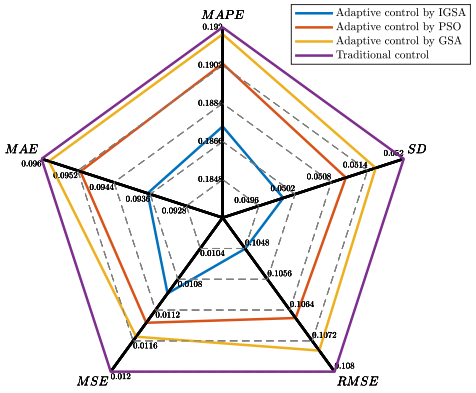

Fig. 16. Frequency control evaluating metrics.

control layer and power control layer. A data-driven adaptive control method is presented by minimizing an improved performance index. The MEE and MSE criteria are combined to construct the improved performance index. The optimal droop control coefficient and virtual inertia gain are then solved by hybrid PSO-GSA technique. Simulation results show that the proposed IGSA based frequency regulation method can regulate frequency quickly and reduce frequency deviation. The proposed IGSA based adaptive control method can be extended to implement short term frequency regulation for gird-connected wind power plants and energy storage systems. This work preliminarily investigates short-term frequency regulation method. In the future work, many significant issues still need to be addressed for power system with PV plants, for example, the real-time performance of the IGSA, frequency stability, load

frequency control, tertiary frequency regulation, and so on.

REFERENCES

[1] M. Obi, R. Bass, "Trends and challenges of grid-connected photovoltaic systems–A review," *Renew. Sust. Energ. Rev.*, vol. 58, pp. 1082-1094, Jan. 2016.

[2] V. R. Vakacharla, et al., "State-of-the-art power electronics systems for solar-to-grid integration," *Sol Energy.*, vol. 210, pp. 128-148, Jul. 2020.

[3] O. Gandhi, et al., "Review of power system impacts at high PV penetration Part I: Factors limiting PV penetration," *Sol Energy.*, vol. 210, pp. 181-201, Aug. 2020.

[4] O. Gandhi, et al., "Review of power system impacts at high PV penetration Part II: Factors limiting PV penetration," *Sol Energy.*, vol. 210, pp. 202-221, Aug. 2020.

[5] R. Rajan, F. M. Fernandez and Y. Yang, "Primary frequency control 1techniques for large-scale PV-integrated power systems: A review," *Renew. Sust. Energ. Rev.*, vol. 144, no. 1, pp. 110998, Apr. 2021.

[6] Y. Liu, et al., "Power control strategy for photovoltaic system based on the Newton quadratic interpolation," *IET Renew. Power Gener.*, vol. 8, no. 6, pp. 611-620, 2014.

[7] E. I. Batzelis, G. E. Kampitsis and S. A. Papathanassiou, "Power reserves control for PV systems with real-time MPP estimation via curve fitting," *IEEE Trans Sustain Energy.*, vol. 8, no. 3, pp. 1269-1280, Jul. 2017.

[8] P. Verma, T. Kaur and R. Kaur, "Power control strategy of PV system for active power reserve under partial shading conditions," *Int. J. Electr. Power Energy Syst.*, vol. 130, pp. 106951, Mar. 2021.

[9] P. Tielens and D. V. Hertem, "The relevance of inertia in power systems," *Renew. Sust. Energ. Rev.*, vol. 55, pp. 999-1009, Dec. 2016.

[10] S. Homan, N. M. Dowell, S. Brown, "Grid frequency volatility in future low inertia scenarios: Challenges and mitigation options," *Appl. Energy.*, vol. 290, pp. 116723, Mar. 2021.

[11] H. B. Yang, et al., "Virtual inertia control strategies for double-stage photovoltaic power generation," *Automation of Electric Power Systems.*, vol. 656, no. 10, pp. 132-147, May. 2019. (in Chinese)

[12] H. D. Sun, et al., "Research on inertia system of frequency response for power system with high penetration electronics," *Proceedings of the CSEE.*, vol. 40, no. 16, pp. 5179-5191, Aug. 2020. (in Chinese)

[13] J. Neely, et al., "Evaluation of PV frequency-watt function for fast frequency reserves," *APEC.*, 1926-1933, 2016.

[14] A. M. Howlader, et al., "Active power control to mitigate voltage and frequency deviations for the smart grid using smart PV inverters," *Appl. Energy.*, vol. 258, pp. 114000, Nov. 2020.

[15] H. Xin, et al., "A new frequency regulation strategy for photovoltaic systems without energy storage," *IEEE Trans Sustain Energy.*, vol. 4, no. 4, pp. 985-993, Oct. 2013.

[16] N. Soni, S. Doolla and M. C. Chandorkar, "Improvement of transient response in microgrids using virtual inertia," *IEEE Trans. Power Deliv.*, vol. 28, no. 3, pp. 1830-1838, Jul. 2013.

[17] D. Feldmann and R. V. D. Oliveira, "Operational and control approach for PV power plants to provide inertial response and primary frequency control support to power system black-start," *Int. J. Electr. Power Energy Syst.*, vol. 127, pp. 106645, Dec. 2021.

[18] A. Fernández-Guillamóna, et al., "Power systems with high renewable energy sources: A review of inertia and frequency control strategies over time," *Renew. Sust. Energ. Rev.*, vol. 118, pp. 109-369, Sep. 2019.

[19] S. I. Nanou, A. G. Papakonstantinou and S. A. Papathanassiou, "A generic model of two-stage grid-connected PV systems with primary frequency response and inertia emulation," *Electr. Power Syst. Res.*, vol. 127, pp. 186-196, Jun. 2015.

[20] C. Zhong, Y. Zhou and G. Yan, "Power reserve control with real-time iterative estimation for PV system participation in frequency regulation," *Int. J. Electr. Power Energy Syst.*, vol. 124, pp. 106367, Jul. 2021.

[21] R. Rajan and F. M. Fernandez, "Power control strategy of photovoltaic plants for frequency regulation in a hybrid power system," *Int. J. Electr. Power Energy Syst.*, vol. 110, pp. 171-183, Mar. 2019.

[22] C. Mu, K. Wang, Z. Ni and C. Sun, "Cooperative differential game-based optimal control and its application to power systems," *IEEE Trans. Ind. Informat.*, vol. 16, no. 8, pp. 5169-5179, Aug. 2020.

[23] C. Mu, Y. Zhang, H. Jia and H. He, "Energy-storage-based intelligent frequency control of microgrid with stochastic model uncertainties," *IEEE Trans. Smart Grid*, vol. 11, no. 2, pp. 1748-1758, March 2020.

[24] C. Mu, W. Liu and W. Xu, "Hierarchically adaptive frequency control for an Ev-integrated smart grid with renewable energy," *IEEE Trans. Ind. Informat.*, vol. 14, no. 9, pp. 4254-4263, Sept. 2018.

[25] W. Liu, G. Geng, Q. Jiang, H. Fan and J. Yu, "Model-free fast frequency control support with energy storage system," *IEEE Trans Power Syst*, vol. 35, no. 4, pp. 3078-3086, July 2020.

[26] L. Guo, et al., "Modeling, analysis and control theory of non-Gaussian random distribution system," *Science Press*, Beijing., 2019.

[27] B. Chen, L. Dang, Y. Gu, N. Zheng and J. C. Príncipe, "Minimum error entropy kalman filter," *IEEE Trans Syst Man Cybern: Systems*, vol. 51, no. 9, pp. 5819-5829, Sept. 2021

[28] B. D. Chen, et al., "Quantized minimum error entropy criterion," *IEEE T Neur Net Lear.*, vol. 30, no. 5, pp. 1370-1380, May. 2019.

[29] Y. M. Ding, et al., "The accuracy and efficiency of GA and PSO optimization schemes on estimating reaction kinetic parameters of biomass pyrolysis," *Energy.*, vol. 176, pp. 582-588, Apr. 2019.

[30] E. Rashedi, E. Rashedi and H. Nezamabadi-pour, "A comprehensive survey on gravitational search algorithm," *Swarm Evol Comput.*, vol. 41, pp. 141-158, Mar. 2018.

[31] S. Nazmul and A. Hojjat, "Gravitational search algorithm and its variants," *Int. J. Patt. Recogn. Artif. Intell.*, vol. 30, no. 8, pp. 1639001, 2016,

[32] A. Naserbegi, Gravitational search algorithm and its variants., "A novel exergy optimization of bushehr nuclear power plant by gravitational search algorithm (GSA)," *Energy.*, vol. 148, pp. 373-385, Feb. 2018.

[33] J. P. Wu, et al., "Analysis on primary frequency regulation of grid-connected PV station in power system," *Electrical Measurement & Instrumentation.*, vol. 53, no. 18, pp. 88-92, Sep. 2016. (in Chinese)

[34] S. Li, "A maximum power point tracking method with variable weather parameters based on input resistance for photovoltaic system," *Energy Convers. Manag.*, vol. 106, pp. 290-299, Oct. 2015.

[35] Q. Jia, et al., "Dynamic coordination mechanism of grid frequency regulation with multiple photovoltaic generation units," *Automation of Electric Power Systems,* vol. 43, no. 24, pp. 59-66, Dec. 2019. (in Chinese)

[36] Northeast regulatory bureau of national energy administration. Grid code for auxiliary service management of grid connected power plants in northeast China. Shenyang, 29th September 2019.

[37] F. Y. Ettoumi, et al., "Statistical analysis of solar measurements in algeria using beta distributions," *Renew. Energ.*, vol. 26, pp. 47-67, 2002.